REPORT DOCUMENTATION PAGE

Form Approved
OMB No. 0704-0188

PLEASE DO NOT RETURN YOUR FORM TO THE ABOVE ORGANIZATION.

1. REPORT DATE *(DD-MM-YYYY)*	2. REPORT TYPE	3. DATES COVERED *(From - To)*
31-03-2009	Final	01-01-2006 - 12-31/2008

4. TITLE AND SUBTITLE
A New Approach for Investigating Crystal Stresses That Drive The Initiation of Fatigue-Induced Defects in Structural Alloys

5a. CONTRACT NUMBER

5b. GRANT NUMBER
FA9550-06-1-0168

5c. PROGRAM ELEMENT NUMBER

6. AUTHOR(S)
Dawson, Paul R.

5d. PROJECT NUMBER

5e. TASK NUMBER

5f. WORK UNIT NUMBER

7. PERFORMING ORGANIZATION NAME(S) AND ADDRESS(ES)
Cornell University
123 Day Hall
Ithaca, New York 14853

8. PERFORMING ORGANIZATION REPORT NUMBER

9. SPONSORING/MONITORING AGENCY NAME(S) AND ADDRESS(ES)
Air Force Office of Scientific Research

10. SPONSOR/MONITOR'S ACRONYM(S)
AFOSR

11. SPONSOR/MONITOR'S REPORT NUMBER(S)
AFRL-AFOSR-VA-TR-2016-0609

12. DISTRIBUTION/AVAILABILITY STATEMENT
Public release.

13. SUPPLEMENTARY NOTES
None.

14. ABSTRACT

We have developed an approach to investigate crystals stresses during cyclic load by coordinating experiments and simulations at the size scale where fatigue induced defects initiate. Our efforts provided new understanding of the stress evolution during cyclic loading through a complementary process between the experimental measurement of lattice strain and the simulation results. The comparison of the experimental and the simulated lattice data culminated in a novel picture of how the stress evolves at the crystal scale. Specifically, using the crystal-based elastoplastic finite element model, we found that for different levels of the single crystal elastic anisotropy, different sets of crystal {hkl}s within a FCC polycrystalline sample evolve differently through the elastic-plastic transition under monotonic tension loading. It is the strength-to-stiffness ratio of these {hkl}s that determines the crystal lattice strain and yield behavior for different values of the single crystal elastic anisotropic ratio. The single crystal elastic anisotropy also causes causes the hysteresis loops under fully-reversed cyclic loading to contract preferentially. For a given average grain size and crystallographic texture, an experimental method for measuring a representative volume element (RVE) in orientation

15. SUBJECT TERMS

16. SECURITY CLASSIFICATION OF:			17. LIMITATION OF ABSTRACT	18. NUMBER OF PAGES	19a. NAME OF RESPONSIBLE PERSON
a. REPORT	b. ABSTRACT	c. THIS PAGE			Paul R. Dawson
U	U	U	UU	14	19b. TELEPHONE NUMBER *(Include area code)* 607-255-3466

Final Report

Grant Title:	**A New Approach For Investigating Crystal Stresses that Drive the Initiation of Fatigue-Induced Defects in Structural Alloys**
Grant Number:	**FA9550-06-1-0168**
Grant Period:	**01/Jan/06 to 31/Dec/08**
PI:	**Paul Dawson**
Co PI:	**Matthew Miller**
Institution	**Cornell University**

Statement of objectives

The principal objective of this project is to develop a more fundamental understanding of the effect of the stress state within crystals and the initiation of fatigue-induced damage in metallic materials. The research consists of a coordinated suite of experiments and simulations to explore how the stress within crystals evolves over the course of a metal's fatigue life. Specifically, our goals are to:

- measure lattice strains by synchrotron x-ray diffraction under dynamic loading conditions using an *in situ* loading/data acquisition system;
- simulate the experiments using highly-resolved virtual polycrystals and a crystal-based elastoplastic finite element model;
- collect microstructural data for the grain morphology, crystallographic texture, and subgrain features such as lattice misorientation and use the data to formulate a digital representation of the material state; and
- develop from the collective results of the experiments, simulations, and characterization a comprehensive understanding of the evolution of crystal stress during cyclic loading and its bearing on the formation of fatigue defects.

The results obtained in this research complement the extensive body of literature on the evolution of microstructure during fatigue and provide an essential, but previously missing, contribution: knowledge of the local stress that drives the formation of defects.

Highlights

We have developed an approach to investigate crystals stresses during cyclic load by coordinating experiments and simulations at the size scale where fatigue induced defects initiate. Our efforts provided new understanding of the stress evolution during cyclic loading through a complementary process between the experimental measurement of lattice strain and the simulation results. The comparison of the experimental and the simulated lattice data culminated in a novel picture of how the stress evolves at the crystal scale.

1. Using the crystal-based elastoplastic finite element model, we found that for different levels of the single crystal elastic anisotropy, different sets of crystal $\{hkl\}$s within a FCC polycrystalline sample evolve differently through the elastic-plastic transition under monotonic tension loading (Figure 1). We show that different sets of crystal $\{hkl\}$s begin yielding at different macroscopic stress levels. It is the strength-to-stiffness ratio of these $\{hkl\}$s that determines the crystal lattice strain and yield behavior for different values of the single crystal elastic anisotropic ratio.
2. The single crystal elastic anisotropy also causes causes the hysteresis loops under fully-reversed cyclic loading to contract preferentially, as shown in the simulation results in Figure 2. It was found that plasticity occurs more readily with continued cycling for certain crystal $\{hkl\}$s than others due to the influence of the strength-to-stiffness ratio as well.
3. For a given average grain size and crystallographic texture, a method for measuring a representative volume element (RVE) in orientation space was developed and applied. For statistical relevance, each diffraction measurement must comprise the response of enough crystals to produce a lattice strain value that is independent of the sample region interrogated and the exact subset of participating crystals for the particular orientation. An example of diffracted image plate data and the required RVE in orientation space is shown in Figure 3.

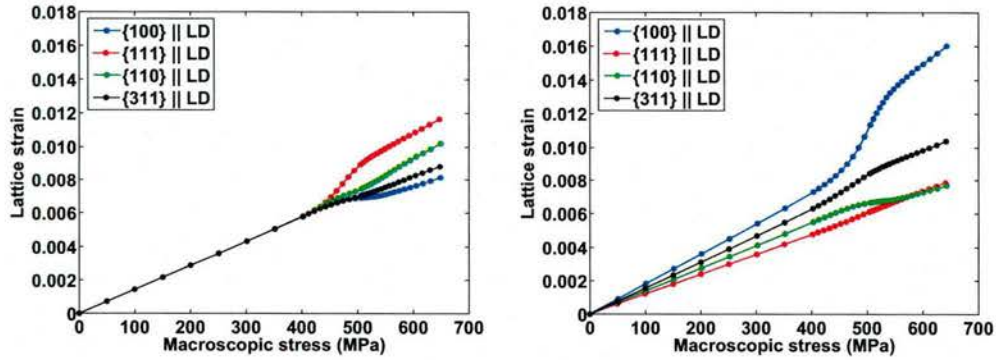

(a) Elastically isotropic FCC single crystals (b) High elastic anisotropy FCC single crystals

Figure 1: The evolution of lattice strains corresponding to different $\{hkl\}$ lattice planes aligned with the loading direction (LD) fibers for low and high single crystal elastic anisotropy.

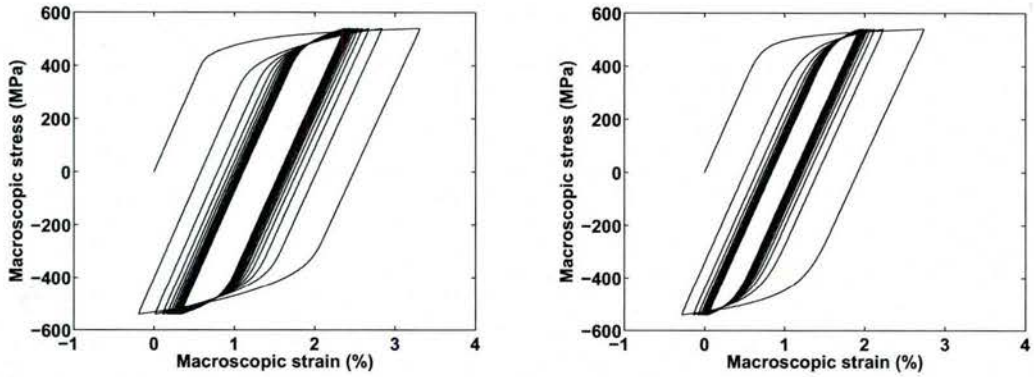

(a) Elastically isotropic FCC single crystals (b) High elastic anisotropy FCC single crystals

Figure 2: Macroscopic stress-strain curve of the virtual polycrystal under uniaxial fully-reversed cyclic loading for 20 cycles

4. The lattice strain data for scattering vectors near the loading direction show a decreasing trend with increasing cycles. The evolution of the lattice strain due to cyclic loading is shown in Figure 4.

5. We have developed an expanded methodology to investigate the evolution of the crystal-level response in polycrystalline metals during cyclic loading. This methodology was developed on AA7075-T6 sheet. The methodology involves comparing the evolving experimental lattice strain directly to the simulation by utilizing the exact fiber geometry found in the experiments. Using this method, we show that the crystal-level mechanical properties such as single crystal elastic anisotropy and yield strength are important in quantifying the stress distribution of polycrystals under cyclic loading.

Completed and expected publications

Results are documented through publications in archival journals. In addition to the paper already published, we plan to publish papers devoted to the highlights listed in the Highlights section above.

1. M.P. Miller, J.-S. Park, P. R. Dawson, and T.-S. Han. "Measuring and modeling distributions of stress state in deforming polycrystals". *Acta Materialia*, 56:3927–3939, 2008.

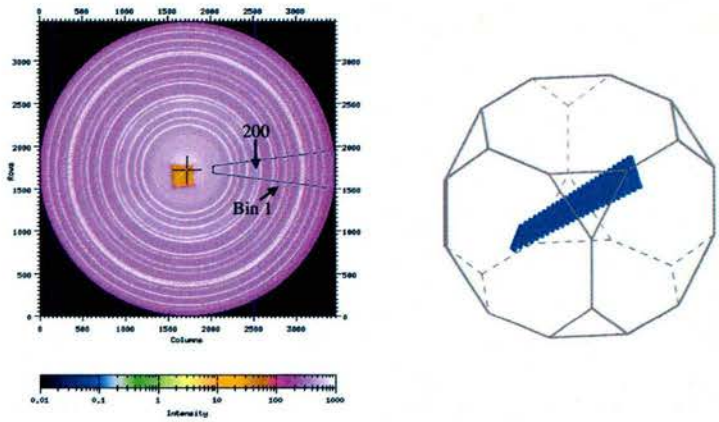

(a) (b)

Figure 3: (a): A typical diffraction pattern for the AA7075-T6 where each ring corresponds to a particular family of crystallographic planes ($\{hkl\}s$) and a 15° azimuthal bin is overlaid. (b): The RVE for the AA7075-T6 is shown, using the Rodrigues parameterization for orientation space, for the {200} for the azimuthal bin indicated in (a). For this particular material the crystals whose orientations fall within the highlighted volume contribute to a single measurement of lattice strain.

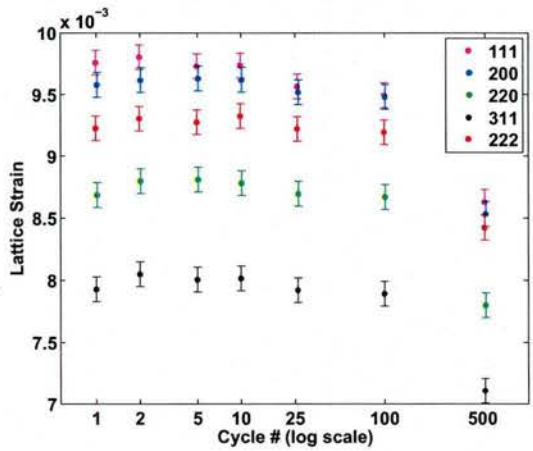

Figure 4: The lattice strain values for all $\{hkl\}s$ are decreasing with increasing cycles for the bin labeled in Figure 3(a). The decrease is largest between 100 and 500 cycles.

2. Su Leen Wong, Paul Dawson. "Influence of elastic anisotropy on the micromechanical behavior of FCC polycrystalline aggregates under uniaxial tensile loading." *In preparation.*

3. Su Leen Wong, Paul Dawson. "On the evolution of the stress distribution of FCC polycrystals during cyclic loading." *In preparation.*

4. Jay Schuren, Matthew Miller. "Experimental determination of a representative volume element in orientation space for lattice strain measured using x-ray diffraction ." *In preparation.*

5. Jay Schuren, Matthew Miller. "Investigating the evolution of experimentally measured lattice strain in AA7075-T6 due to cyclic loading." *In preparation.*

6. Jay Schuren, Su Leen Wong, Matthew Miller, Paul Dawson. "Combining simulation and experiments to measure the evolution of the stress at the crystal scale during cyclic loading." *In preparation.*

Remaining work

The current project constitutes the PhD research of two graduate students: Su Leen Wong and Jay Schuren. The research will be expanded upon and will culminate in their dissertations. Their goal is to improve the understanding between the evolution of crystal stresses and the micromechanics that lead to fatigue defect initiation.

We are in the process of reducing the lattice strain data from our most recent experiment conducted in March 2009. The results for many scattering vectors will provide a more complete picture on the source of the evolution of the lattice strain data: are the crystal stress tensors rotating or changing in magnitude?

We will compare experiment and simulation lattice strains under zero-tension cyclic loading using the methodology described in the previous section to develop an understanding of the evolving stress state with respect to the vertices of the yield surface. The measured lattice strain will be compared directly to the simulation by utilizing the same fiber geometry as in the experiments. We also plan to use the concept of the strength-to-stiffness ratio, to examine its influence on the evolution of lattice strains and cyclic hardening during zero-tension loading.

Details of accomplishments

1. Elastic anisotropy parametric study

A suite of simulations was conducted using a crystal-based finite element model for uniaxial tensile loading and fully-reversed cyclic loading. The single crystal elastic anisotropic ratio was varied systematically to examine its influence on the crystal-level behavior of the virtual polycrystal.

A virtual polycrystal in the shape of a cube, as shown in Figure 12, is instantiated with 1098 rhombic dodecahedra grains although there are additional partial grains that make up the surfaces of the cube. A rhombic dodecahedral grain has 12 faces and consists of 48 10-node tetrahedra finite elements each assigned the same initial lattice orientation. The initial orientations of all the grain are randomly assigned from a uniform orientation distribution function (ODF). The orientations of the finite elements that constitute a grain are allowed to evolve independently as the deformation proceeds. We consider FCC crystals which deform by crystallographic slip on $\{111\}$ slip planes in $\langle 110 \rangle$ slip directions. This finite element mesh that was generated consists of 81000 finite elements and is used in all the simulations in this study.

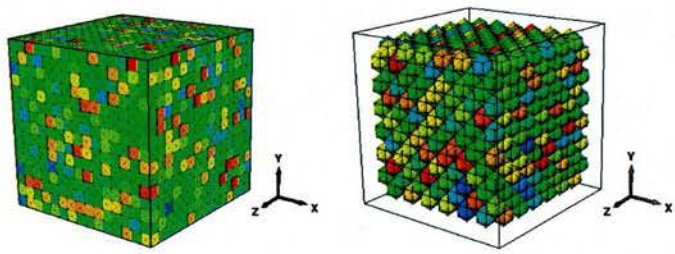

(a) (b)

Figure 5: (a): Virtual polycrystal in the shape of a cube including partial surface grains. (b): Interior of virtual polycrystal showing complete rhombic dodecahedra grains

The elastic anisotropy of a single crystal arises from the orientation dependence of the elastic response of the crystal lattice. The level of elastic anisotropy of a single crystal with cubic symmetry is quantified by the ratio of the elastic stiffness in the $\langle 111 \rangle$ crystal direction to the elastic stiffness in the $\langle 100 \rangle$ crystal direction, and it is defined as the elastic anisotropic ratio, $r_E = E_{\langle 111 \rangle}/E_{\langle 100 \rangle}$. In cubic crystals, the $\langle 111 \rangle$ direction is typically the stiffest direction and the $\langle 100 \rangle$ direction is the most compliant direction. In this study, we are interested in the crystal level response when the elastic anisotropy ratio (r_E) is varied, while keeping the average macroscopic elastic response of the virtual polycrystal constant. A range of r_Es was chosen to represent single crystal behavior ranging from an isotropic single crystal ($r_E = 1.0$) to a highly anisotropic single crystal ($r_E = 3.0$). The macroscopic stress-strain response is shown in Figure 6 for $r_E = 1.0$ and $r_E = 3.0$. The single crystal elastic moduli were varied systematically while keeping the macroscopic Young's modulus (slope of the elastic portion of the macroscopic stress-strain curve) constant for all values of r_E under consideration. The Young's modulus of the macroscopic stress-strain curves shown in Figure 6 is the same as the Young's modulus for pure aluminum.

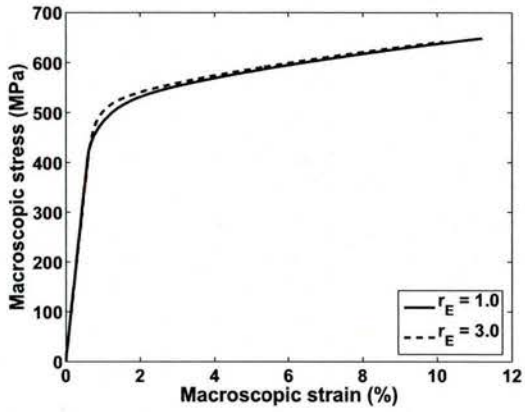

Figure 6: Macroscopic true stress-strain curve under uniaxial tensile loading for $r_E = 1.0$ and $r_E = 3.0$.

The set of all crystals with the $\{hkl\}$ lattice plane normal aligned with the loading direction (LD) is referred to as the $\{hkl\}$ || LD crystallographic fiber. The average lattice strain and plastic strain rate magnitude under uniaxial tensile loading are examined for different $\{hkl\}$ || LD fibers. In this suite of simulations, the same finite element mesh is used and all slip system hardening parameters are kept constant. The evolution of the lattice strains through the elastic-plastic transition for two different values of the single crystal anisotropic ratio, $r_E = 1.0$ and $r_E = 3.0$ are shown in Figure 7. The plastic strain rate magnitudes corresponding to different $\{hkl\}$ || LD fibers are shown in Figure 8. A large nonlinear increase in the magnitude of the plastic strain rate indicates that on average, crystals belonging to the $\{hkl\}$ || LD fiber have yielded.

The lattice strains corresponding to the elastically isotropic case ($r_E = 1.0$) are shown in Figure 7(a) and it shows that the lattice strains are the same for all fibers in the elastic regime, a result that is consistent with an elastically isotropic material. Once yielding begins and plastic deformation occurs, the lattice strains diverge in the plastic regime. The $\{111\}$ lattice strains rise above the other $\{hkl\}$ lattice strains in the post-yield regime. This is accompanied by the $\{hkl\}$ || LD fiber yielding at a higher macroscopic stress compared to the other fibers as seen in Figure 8(a). Although all the crystals are elastically isotropic, Figure 8(a) demonstrates that there is plastic or yield strength anisotropy as well because different crystallographic fibers yield at different macroscopic stress levels.

When the elastic anisotropic ratio r_E is increased to $r_E = 3.0$, the behavior of the crystals are influenced by a combination of the elastic and plastic anisotropy and this results in different behaviors in both the elastic and plastic regime. The lattice strains corresponding to the high elastic anisotropy case

($r_E = 3.0$) are shown in Figure 7(b). It can be seen that the single crystal elastic anisotropy results in a spread between the lattice strains for different $\{hkl\}$s in the elastic regime. In the post-yield regime, the magnitude of the $\{111\}$ lattice strains decreases while the $\{100\}$ lattice strains rise above the others for $r_E = 3.0$, as seen in Figure 8(b). This observation is accompanied by the $\{100\}$ fiber yielding at a higher macroscopic stress level compared to the $\{111\}$ fiber, which is the reverse of what is observed in the elastically isotropic case ($r_E = 1.0$).

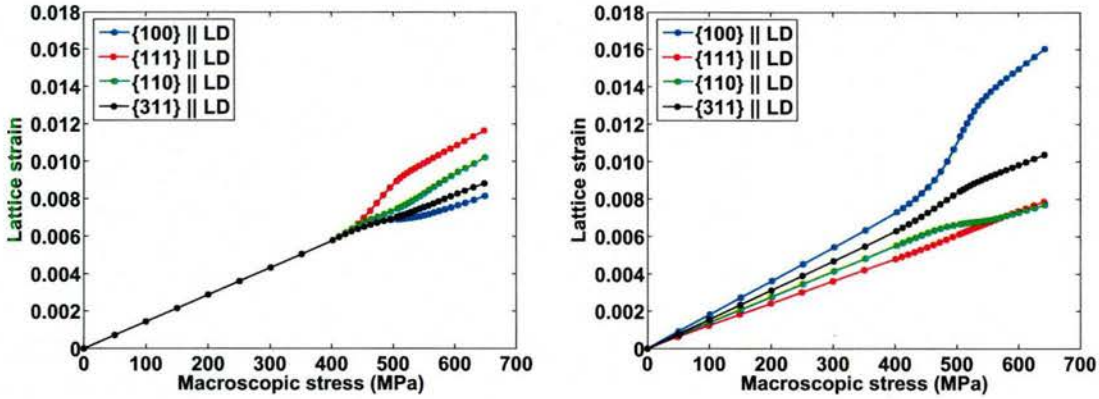

(a) $r_E = 1.0$ (b) $r_E = 3.0$

Figure 7: The evolution of the lattice strains through the elastic-plastic transition corresponding to different $\{hkl\}$ || LD fibers for $r_E = 1.0$ and $r_E = 3.0$. Uniaxial tensile loading is applied to the virtual polycrystal specimen.

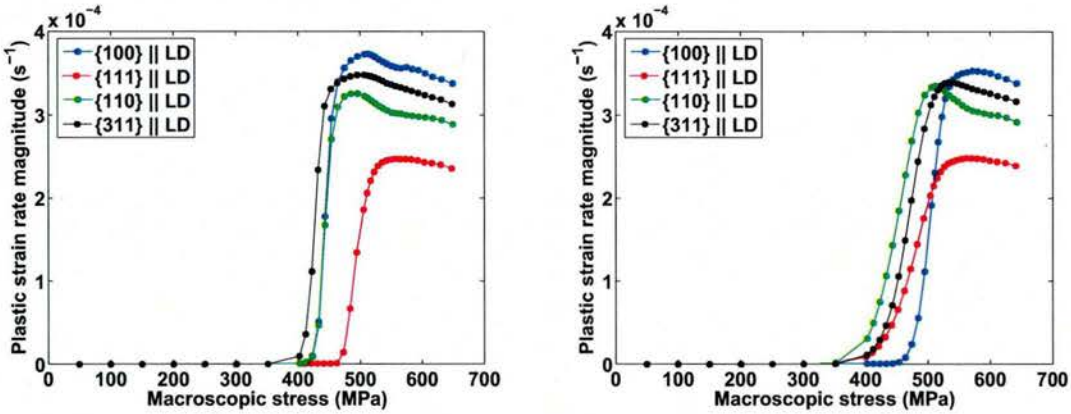

(a) $r_E = 1.0$ (b) $r_E = 3.0$

Figure 8: The magnitude of the plastic strain rate as a function of the macroscopic stress corresponding to different $\{hkl\}$ || LD fibers for $r_E = 1.0$ and $r_E = 3.0$. Uniaxial tensile loading is applied to the virtual polycrystal specimen.

The evolution of orientation-dependent lattice strain and plastic strain rate magnitude seen in Figures 7-8 indicate that these behaviors are influenced by the elastic and plastic properties of a crystal. The orientation dependence of the elastic and plastic behavior of a single crystal can be quantified using the strength-to-stiffness ratio (r^S), which is the ratio of the plastic strength to the elastic stiffness of a single

crystal in a particular $\langle hkl \rangle$ direction. The strength-to-stiffness ratio for a given $\langle hkl \rangle$ crystal direction is defined as:

$$r^S_{\langle hkl \rangle} = \frac{m_{\langle hkl \rangle}}{E_{\langle hkl \rangle}} \tag{1}$$

where $m_{\langle hkl \rangle}$ is the orientation-dependent Schmid factor and $E_{\langle hkl \rangle}$ is the directional Young's modulus for a cubic single crystal under uniaxial tension in the direction $\langle hkl \rangle$. The Schmid factor $m_{\langle hkl \rangle}$ is the maximum resolved shear stress on all the slip systems of a crystal under a uniaxial stress state applied in a particular $\langle hkl \rangle$ direction.

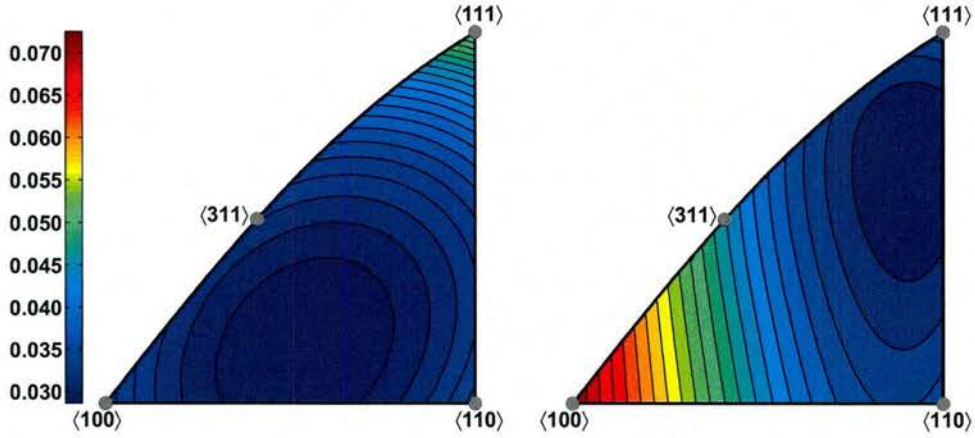

(a) $r_E = 1.0$ (b) $r_E = 3.0$

Figure 9: FCC single crystal strength-to-stiffness ratio, $r^S_{\langle hkl \rangle}$ over the fundamental orientation triangle

Since both the elastic stiffness and the Schmid factor vary with orientation, the strength-to-stiffness ratio $r^S_{\langle hkl \rangle}$ also varies with orientation. Figure 9 depicts the plots of $r^S_{\langle hkl \rangle}$ over the fundamental orientation triangle corresponding to two levels of the elastic anisotropic ratio r_E. The elastically isotropic case ($r_E = 1.0$) leads to the highest strength-to-stiffness for the $\langle 111 \rangle$ crystal direction and that influences that $\{111\}$ fiber to yield at a higher macroscopic stress level as seen in Figure 8(a). The high elastic anisotropy case ($r_E = 3.0$) however, has the highest strength-to-stiffness for the $\langle 100 \rangle$ crystal direction instead which corresponds to the $\{100\}$ fiber yielding at a relatively higher macroscopic stress level compared to the other $\{hkl\}$s, as seen in Figure 8(b). Therefore, the strength-to-stiffness ratio determines the order in which the crystals begin yielding. The lattice strains also begin deviating from a linear elastic response, shown in Figure 7 once yielding begins because the yield behavior is determined by the strength-to-stiffness $r^S_{\langle hkl \rangle}$.

We also examine the influence of the single crystal elastic anisotropy r_E on the macroscopic and crystal-level behavior of the virtual polycrystal under uniaxial fully-reversed cyclic loading for 20 complete cycles. The same finite element mesh and slip hardening parameters used in the uniaxial tensile loading simulations are used in the fully-reversed cyclic loading simulations as well. It is observed that the single crystal elastic anisotropy influences the contraction of the hysteresis loops with increasing cycles, shown in Figure 10. The macroscopic stress-strain curve for the high elastic anisotropy case ($r_E = 3.0$) collapses more rapidly compared to the elastically isotropic case ($r_E = 1.0$). The magnitude of the plastic strain rate vector at the maximum macroscopic stress level on each cycle is also shown in Figure 11 for different fibers. It is observed that plasticity occurs more readily for certain $\{hkl\}$s than others. For the $r_E = 1.0$ case, the $\{100\}$ || LD fiber continues to be active in terms of plasticity throughout the deformation while the plastic strain rate of the $\{111\}$ || LD fiber decreases relatively quickly after 20 cycles. For the $r_E = 3.0$ case however, the $\{100\}$ || LD fiber decreases at a much faster rate compared to the other sets of crystals and after 20 cycles, the $\{111\}$ || LD fiber instead are experiencing more plastic straining compared to

the {100} || LD fiber. These trends show that the strength-to-stiffness ratio plays an important role in influencing the plastic response of the polycrystal under fully-reversed cyclic loading.

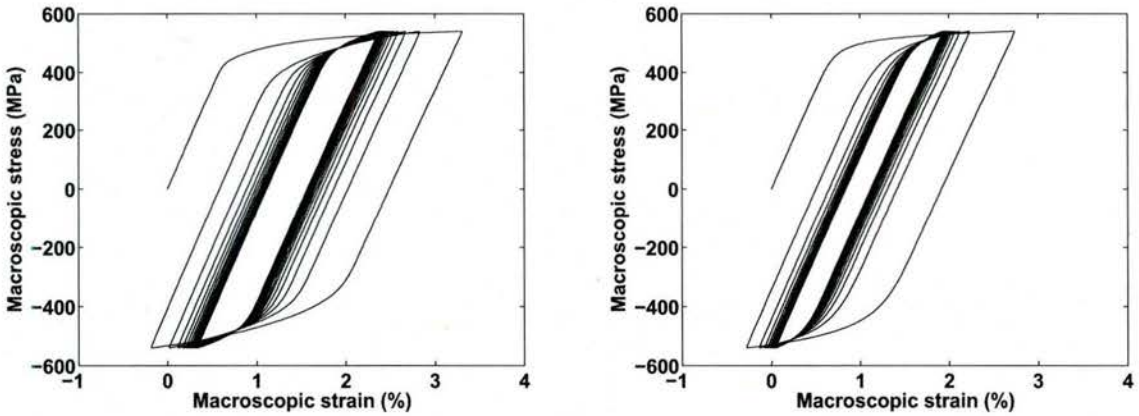

(a) $r_E = 1.0$ (b) $r_E = 3.0$

Figure 10: Macroscopic stress-strain curve of the virtual polycrystal under uniaxial fully-reversed cyclic loading for 20 cycles

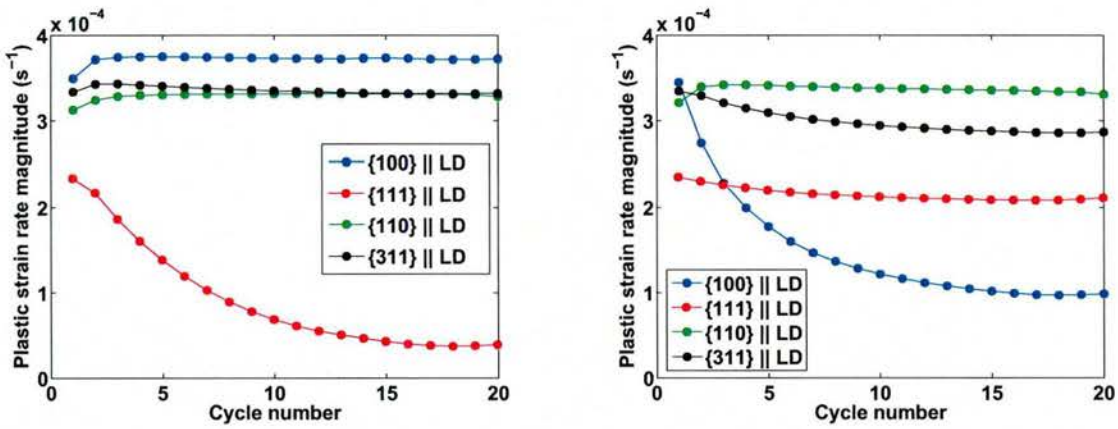

(a) $r_E = 1.0$ (b) $r_E = 3.0$

Figure 11: Magnitude of the plastic strain rate vector at the maximum macroscopic stress on each cycle for two levels of single crystal elastic anisotropy

2. Quantifying experimental lattice strains

Cycle-by-cycle variation in the lattice strain is linked to the evolution of the stress tensor at the crystal scale. To quantify the stress that drives the initiation of fatigue induced defects we must first understand both the amount of variation and the statistical significance of the results.

The measurement-by-measurement resolution of the lattice strain is governed by the determination of diffracted peak positions and the application of a geometric model to correct for the non-orthogonality of the detector with respect to the incoming x-ray. The metric for gaging the quality of the corrected data is based on the peak positions of a calibrant material, cerium dioxide in this case, which is added to one side of the specimen. This calibrant has a known lattice parameter and the diffraction pattern should

appear as perfect concentric circles. Through quantifying any deviation from circular we can obtain a value for the resolution of the experiment.

Figure 12 outlines the process of determining the resolution in terms of 2θ, where θ is the Bragg angle. The first panel depicts an example of image plate data with two diffracted calibrant rings. By dividing the rings into equal angular bins and determining the peak positions, we can generate plots of the angular position versus the particular η bin. The angular difference between the experimental peak position and the theoretical peak position generated using the lattice parameter establishes the resolution of the lattice strain. The conversion of $\Delta 2\theta$ to a strain value for a given $\{hkl\}$ is achieved using Bragg's law, $\lambda = 2d_{hkl} \sin \theta_{hkl}$, to find the limiting strain resolution $(\Delta d/d)$.

The definition of a representative volume element (RVE) for diffraction measurements is different from the classical definition because only a subset of crystals within the irradiated volume of the sample diffract. These diffracting crystals share a common orientation to within a rotation about the plane normal of the crystal. The relationship is defined as:

$$\mathbf{Rc} = \pm\mathbf{q} \tag{2}$$

where $\mathbf{R}$ is the crystal orientation, $\mathbf{c}$ is the diffracting family of lattice planes, and $\mathbf{q}$ is the bisector of the incoming and diffracted x-ray as shown in Figure 13. All orientations ($\mathbf{R}$) that satisfy Equation 2 fall along a fiber. Employing a Rodrigues parameterization of orientation space the fiber is a line.

A RVE for lattice strain measurements is defined to have enough crystals diffracting to produce a statistically significant response. The lattice strain measurement must be orientation dependent and insensitive to the exact subset of crystals interrogated. For a given grain size and texture the geometry of the fiber can be adjusted to dictate the approximate number of crystals participating in the diffraction experiment. Experimentally this is controlled by two parameters: the azimuthal bin size (η range) and a sample oscillation about a prescribed value (rocking). An azimuthal bin of 15° is overlaid on image plate data in Figure 14(a). Rocking is the slight reorientation of the sample during the diffraction measurement achieved by a 2° rotation about an axis through the sample. The combination of the diffracted signal from these two angular ranges is a fiber with a specific geometry in orientation space. For the {200} peak the corresponding fiber is shown in Figure 14(b). The length is along the direction of the fiber, the width is defined by the azimuthal bin size, and the thickness comes from the 2° rocking. Understanding the connection between the fiber dimensions and the number or participating crystals is essential for measuring statistically significant lattice strain values in the AA7075-T6. When the fiber dimensions are less than the needed size for a RVE, neighborhood effects would govern the results.

The determination of the RVE is also linked to the crystallographic multiplicity. Multiplicity is a measure of the likelihood that a given $\{hkl\}$ will diffract with respect to another. For cubic materials the lowest multiplicity crystallographic family corresponds to the cube face with six possible permutations that would appear identical to diffraction techniques. For a weak texture, as is the case for the AA7075-T6, the number of crystals participating in a diffraction measurement of each $\{hkl\}$ will scale with the multiplicity(i.e. $M_{311} = 24$ and $M_{200} = 6$). Therefore the limiting $\{hkl\}$ in the AA7075-T6 is the {200} which establishes the volume of the fiber necessary to measure the most likely response of crystals lying along a particular fiber in orientation space (statistically significant).

To determine whether a RVE contains enough crystals we utilize specimen symmetry with resepect to the loading axis. This symmetry is visible in the {200} lattice strain data shown in Figure 15(a). Initially at $\eta = 0°$ the scattering vector is as close to the loading direction as possible producing the maximum lattice strain value. As the azimuthal angle increases the lattice strain will decrease to a minimum at $\eta = 90°$ (near the transverse direction). Due to specimen symmetry, the lattice strain measured at $\eta = 0°$ must be statistically similar to the measurement at $\eta = 180°$. Figure 15(b) depicts the fibers corresponding to $\eta = 0°$ and $\eta = 180°$, as shown by the blue and red fibers respectively. The difference in the two fibers indicates that the participating crystals are two distinct subsets, but the mechanical response must be similar.

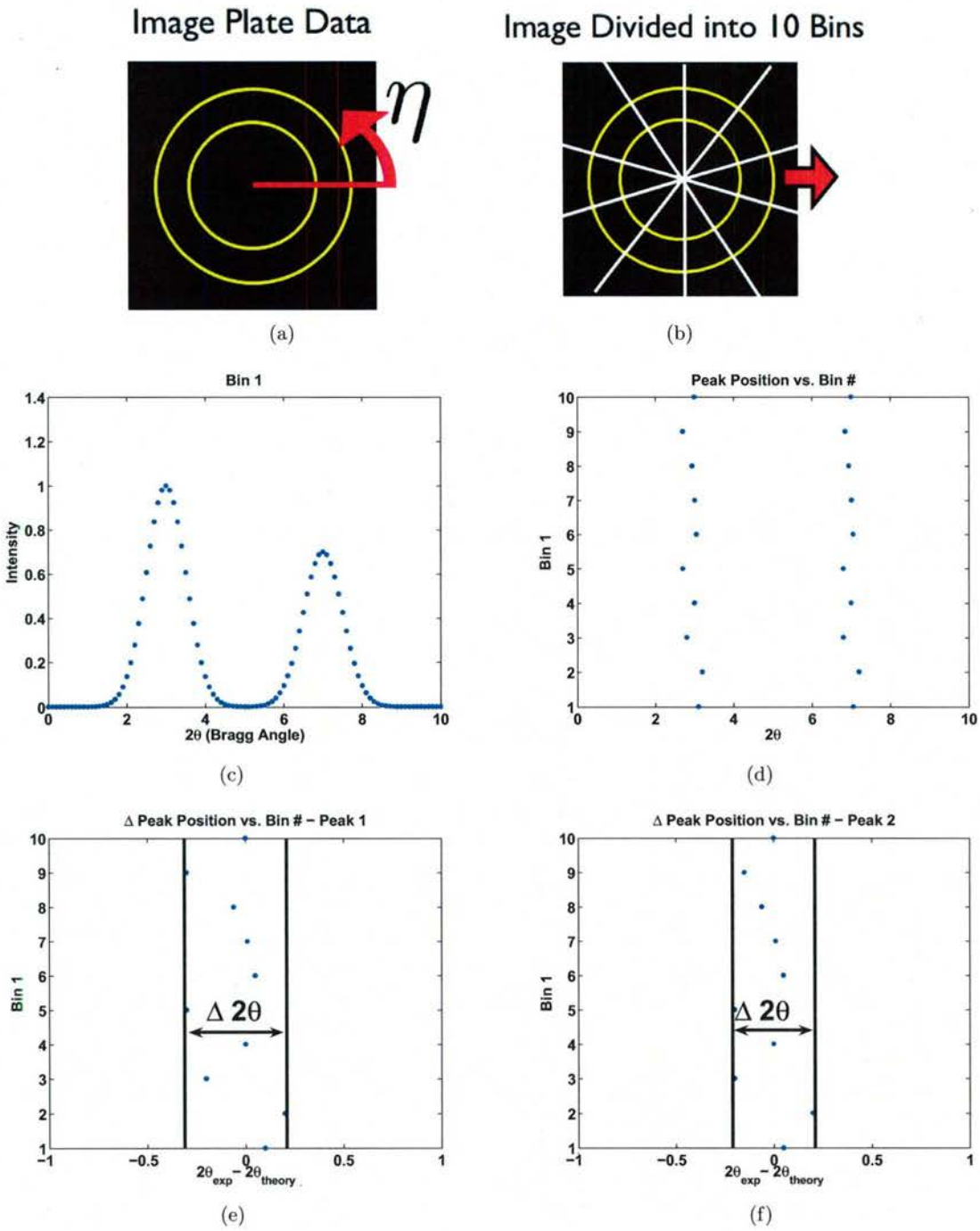

Figure 12: The method for determining the lattice strain resolution of image plate data. A peak located at $2\theta = 7^\circ$ with $\Delta 2\theta = 0.001^\circ$ leads to a strain resolution of approximately 1.4×10^{-4}.

Application of these methods for the bin labeled in Figure 14(a) leads to the lattice strain results in Figure 16. Figure 16(a) shows lattice strain results versus the macroscopic stress for the first cycle. The material deforms elastically from 0 to ~400 MPa as shown by the near constant slope for each $\{hkl\}$. The

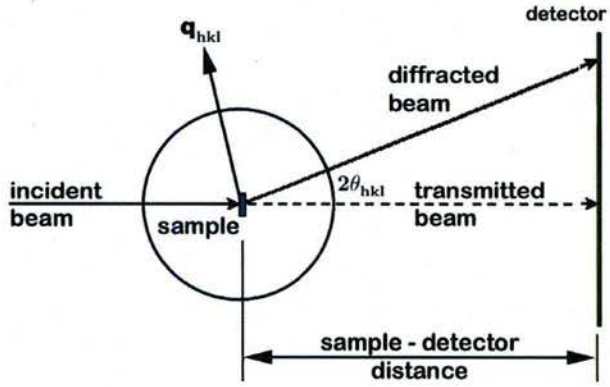

Figure 13: Two-dimensional schematic showing the relationship between the specimen, detector, scattering vector ($\mathbf{q_{hkl}}$), intersecting a sphere corresponding to the strain pole figure surface, and the incident and diffracted beams. The value θ_{hkl} is the Bragg angle for a particular $\{hkl\}$.

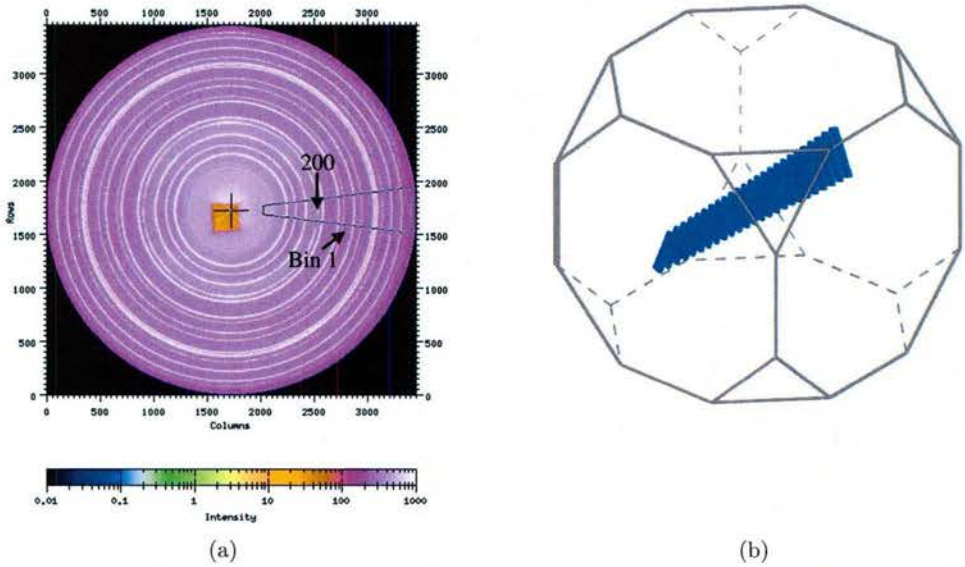

(a) (b)

Figure 14: (a): A typical diffraction pattern for the AA7075-T6 with the cerium dioxide calibrant where each ring corresponds to a particular family of crystallographic planes ($\{hkl\}s$) and a 15° azimuthal bin is overlaid. (b): The 200 fiber bundle for the azimuthal bin indicated in (a) shown in orientation space. The crystals whose orientations fall within the highlighted volume contribute to a single measurement of lattice strain.

relative order of the $\{hkl\}s$ in the elastic regime arises from the single crystal anisotropy and the angle of co-axiality of the scattering vector and the loading direction. The decrease in the angle of co-axiality between the scattering vector and the loading direction governs the decrease between the $\{111\}$ and the $\{222\}$ lattice strains.

Figure 16(b) shows the lattice strain vs. the log cycle for the bin labeled in Figure 14(a). Diffraction

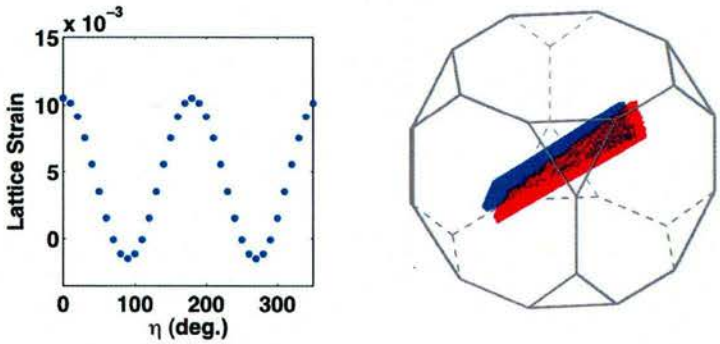

(a) (b)

Figure 15: (a): The {200} lattice strain values as a function of the azimuthal angle. Specimen symmetry can be seen by comparing the maximum values at $\eta = 0°$ and 180°. (b): The blue and red fibers in orientation space correspond to the {200} fibers for 15° azimuthal bins centered about $\eta = 0°$ and 180°.

measurements were made after cycles 1, 2, 5 10, 25, 100, and 500. The specimen failed after approximately 800 cycles. The decrease in the lattice strain values between cycle 100 and cycle 500 is much larger than the experimental resolution. This decrease in the lattice strain for all $\{hkl\}s$ is a response to the evolution of the stress with increasing cycle. Currently we have only investigated the cyclic data in this particular azimuthal bin since the experiment was conducted during our Spring '09 beam time at the Cornell High Energy Synchrotron Source. This measurable lattice strain evolution is a strong indicator that we are capturing the effects of the changing micromechanical state due to cyclic loading. The results for other scattering vectors will provide a more complete picture of what is happening at the crystal scale; enabling us to investigate hypotheses like: is the stress slightly rotating toward a vertex of the yield surface with each cycle?

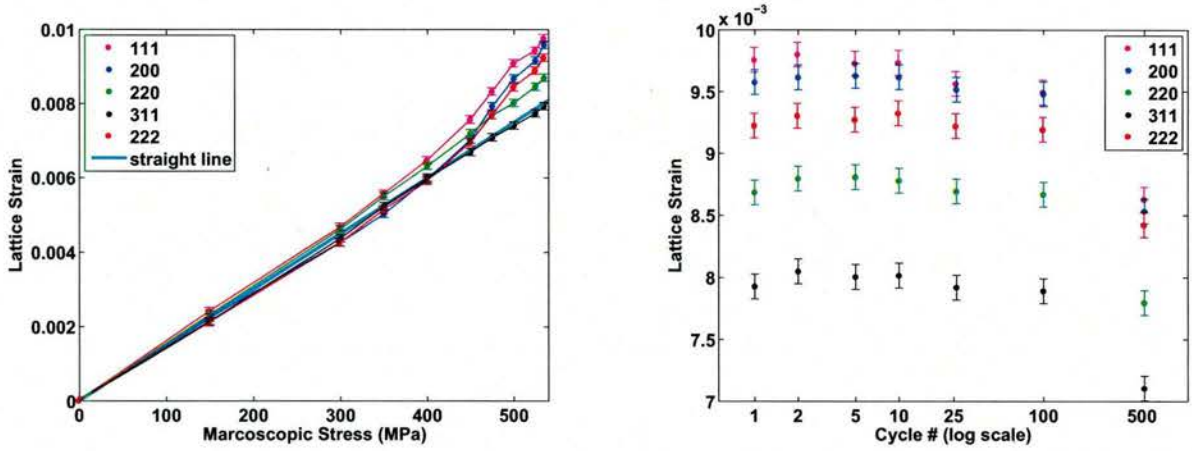

(a) (b)

Figure 16: a: Lattice strain versus the macroscopic stress for the azimuthal bin shown in Figure 14(a). b: The lattice strain values for all $\{hkl\}s$ are decreasing with increasing cycles. The decrease is largest between 100 and 500 cycles.

3. Expanded methodology for comparing experiments and simulations

An expanded methodology has been developed to enable a direct comparison between x-ray diffraction measurements and crystal-based finite element simulations during cyclic loading. The AA7075-T6 aluminum alloy has been used to develop this methodology but this methodology can be used to investigate the crystal-level response of other types of polycrystalline metals as well. The steps of this procedure are as follows:

1. Instantiate the virtual specimen
   A virtual polycrystal specimen is created with rhombic dodecahedral grains discretized with 48 elements per grain. The ODF of the virtual specimen is identical to the physical specimen.

2. Determine the strain hardening parameters
   Using an crystal-based elastoplastic finite element model, the appropriate strain hardening parameters for the virtual specimen are determined by matching the macroscopic stress-strain curve from the experiment with the simulation results.

3. Determine the single crystal elastic moduli on first cycle
   Although the macroscopic stress-strain response can be matched between the experiment and simulation, there also needs to be agreement between the experiment and simulation at the crystal level. The single crystal elastic moduli are determined by comparing computed lattice strains with the measured lattice strains on the first cycle using the same scattering vectors as in the experiment. The single crystal elastic anisotropy is varied until a reasonably accurate match is achieved.

4. Compare lattice strains on successive cycles
   Once the single crystal elastic moduli have been determined, we can quantify the evolution of the stress/strain distribution of the crystals on successive cycles.